

# Constraining cosmology with $N$ -body simulations for future spectroscopic galaxy surveys at $2 \leq z \leq 3$

Sy-Yun Pu,<sup>1,2,\*</sup> Teppei Okumura,<sup>1,3,†</sup> Chian-Chou Chen,<sup>1,‡</sup> Takahiro Nishimichi,<sup>4,5,3</sup> and Kazuyuki Akitsu<sup>6</sup>

<sup>1</sup>*Academia Sinica Institute of Astronomy and Astrophysics (ASIAA), No. 1, Section 4, Roosevelt Road, Taipei 106216, Taiwan*

<sup>2</sup>*Institute of Astronomy and Department of Physics, National Tsing Hua University, Hsinchu 30013, Taiwan*

<sup>3</sup>*Kavli IPMU (WPI), UTIAS, The University of Tokyo, Kashiwa, Chiba 277-8583, Japan*

<sup>4</sup>*Department of Astrophysics and Atmospheric Sciences, Faculty of Science, Kyoto Sangyo University, Kyoto 603-8555, Japan*

<sup>5</sup>*Center for Gravitational Physics and Quantum Information, Yukawa Institute for Theoretical Physics, Kyoto University, Kyoto 606-8502, Japan*

<sup>6</sup>*Theory Center, Institute of Particle and Nuclear Studies, High Energy Accelerator Research Organization (KEK), Tsukuba, Ibaraki 305-0801, Japan*

(Dated: August 1, 2025)

Determining the spatial curvature ( $\Omega_k$ ) independent of cosmic microwave background observations plays a key role in revealing the physics of the early universe. The Hubble tension is one of the most serious issues in modern cosmology. We investigate halo catalogs identified from  $N$ -body simulations at  $z = 2$  and 3, mimicking high-redshift galaxy surveys. We measure redshift-space correlation functions of halos from the two snapshots. We detect clear features of baryon acoustic oscillations and redshift-space distortions. We find that we can obtain a few percent constraints on both the geometric distances and growth of structure at the distant universe in future surveys. By taking into account the information of the underlying matter power spectrum, we demonstrate that we can also achieve constraint on the Hubble constant  $H_0$  with a few percent as well as the spatial curvature with  $|\Omega_k| \lesssim 0.1$  by observing galaxies with the number density with  $\bar{n}_g \simeq 10^{-4} (h^3 \text{ Mpc}^{-3})$ . Our analysis provides a timely forecast for the upcoming spectroscopic surveys, which target emission line galaxy or dusty star-forming galaxy samples.

*Introduction.* Cosmological models have been tested via various observations including cosmic microwave background (CMB) [1, 2], gravitational lensing [3, 4], galaxy redshift surveys [5–7], Type-Ia supernovae [8, 9], etc. Cold dark matter with a cosmological constant, the  $\Lambda$ CDM model, has successfully explained all of these observations so far. However, there exist discrepancies between some parameters determined from the early and local universe, known as the Hubble tension [10] and the  $S_8$  tension [11]. The Dark Energy Spectroscopic Instrument (DESI) [12–14], the latest galaxy survey, reported cosmological constraints that support dynamical dark energy with  $w > -1$ . However, combining them with other datasets still includes the cosmological constant ( $w = -1$ ) within  $2\sigma$  in a large cosmological parameter space [15]. Although the geometry of the universe has been found flat by the CMB, the flatness of the universe has not been constrained in late universe observations [16–20]. One way to tackle these issues is to extend the observations of cosmological objects to the more distant universe [21]. Cosmological spectroscopic experiments at  $z \gtrsim 2$  have the potential to put meaningful constraints on curvature [16], neutrino mass [22, 23], inflation [22], and dark energy [24].

Indeed, in the coming years a number of optical and near-infrared facilities in plan aim to conduct large-scale

cosmological spectroscopic surveys for the  $z \sim 2 - 4$  Universe, including the Subaru Prime Focus Spectrograph [PFS; 25], DESI-II, Stage-V experiments such as Maunakea Spectroscopic Explorer [MSE; 26], MegaMapper [27], and SpecTel [28]. In the longer wavelength regime, the 50-m single-dish submillimeter telescope AtLAST plans to perform the first cosmological spectroscopic surveys for over 100,000 galaxies in (sub)millimeter in degree square scales [29].

The galaxy populations that these future facilities will target include Lyman Alpha Emitters (LAEs), Lyman Break Galaxies (LBGs), and dusty star-forming galaxies (DSFGs), and they are shown to probe halo masses that differ by up to two orders of magnitude, from  $\sim 10^{11} M_\odot$  by the LAEs [30] to  $\sim 10^{13} M_\odot$  by the DSFGs [31, 32]. The combined measurements of the various galaxy populations, therefore, allow us to suppress the cosmic variance via the multi-tracer technique [33, 34]. Many forecasts have been made for such tracers to test the precision of upcoming and future cosmological surveys including the PFS [25, 35], the Euclid space telescope [36], MegaMapper, MSE and MUltiplexed Survey Telescope (MUST) [37]. However, the cosmological forecasts were based on the Fisher matrix formalism, and thus the expected constraints would be too optimistic. It is necessary to utilize mock catalogs to provide more realistic forecasts.

In this paper, using dark matter  $N$ -body simulations run assuming a spatially-flat  $\Lambda$ CDM model [2], we aim to provide a first forecast on the cosmological constraints via clustering measurements that will be enabled by future spectroscopic surveys. As a first step, we focus on

\*Electronic address: psyn@gapp.nthu.edu.tw

†Electronic address: tokumura@asiaa.sinica.edu.tw

‡Electronic address: ccchen@asiaa.sinica.edu.tw

TABLE I: Properties of mock halo catalogs. The second column shows the mass range of the halos,  $\bar{M}_h$  is the average mass and  $\bar{n}_g$  is the number density.

$z$	$\log M_h / (h^{-1} M_\odot)$	$\log \bar{M}_h / (h^{-1} M_\odot)$	$10^4 \bar{n}_g$ ( $h^3 \text{ Mpc}^{-3}$ )
2	11.5 – 12.0	11.7	32.2
	12.5 – 13.5	12.8	4.05
3	11.5 – 12.5	11.9	26.8
	12.5 – 13.5	12.7	1.02

redshifts of 2 and 3, a natural extension of current state-of-the-art measurements [12]. For each snap shot, we construct two dark-matter halo samples with higher and lower number densities, which roughly correspond to the PFS ELG survey [25] and the AtLAST [29], respectively. We measure the correlation functions of dark-matter halos from the two snapshots. We then discuss how much cosmological information can be extracted from baryon acoustic oscillations (BAO) and redshift-space distortions (RSD) as well as the shape of the underlying matter power spectrum. We investigate how strongly the cosmological parameters can be constrained, including the spatial curvature ( $\Omega_k$ ) and Hubble constant ( $H_0$ ) from observations at such a high-redshift universe.

*N-body Simulations and halo catalogs.* We use  $N$ -body simulations run as part of an extension of the DARK QUEST project [38]. We employ  $3000^3$  dark matter particles of mass  $m_p = 2.584 \times 10^{10} h^{-1} M_\odot$  in a cubic box on the side  $2h^{-1}\text{Gpc}$ . We have the data set from three independent realizations and we specifically analyze clustering of dark matter halos of the snapshots at  $z = 2$  and  $z = 3$ . Halos are identified using the ROCKSTAR algorithm [39]. Their velocities and positions are determined by the average of the member particles within the innermost 10% of the subhalo radius. The halo mass,  $M_h$ , is defined by a sphere with radius within which the enclosed average density is 200 times the mean matter density.

The statistical properties of halos that host galaxies at high redshifts, such as dusty galaxies and emission line galaxies, have not been accurately determined yet by observations. In this paper, thus, we do not consider any specific galaxy population but use all subhalos with some mass range. In order to see the halo mass dependence of the cosmological results, we adopt two mass ranges as shown in Table I, referred to as the low- and high-mass samples, roughly corresponding to the mass ranges of emission line galaxies ( $\sim 10^{-3} [h^3 \text{ Mpc}^{-3}]$ ) [25] and dusty galaxies ( $\sim 10^{-4} [h^3 \text{ Mpc}^{-3}]$ ) [29], respectively.

*Measurements of redshift-space correlation functions.* From the simulations, we measure the redshift-space correlation functions of halos,  $\xi(r, \mu_r)$ , where  $r = |\mathbf{r}|$  with  $\mathbf{r}$  being the separation vector between two points and  $\mu_r$  is the direction cosine between the line of sight and  $\mathbf{r}$ . We then determine the multipole moments of the correlation

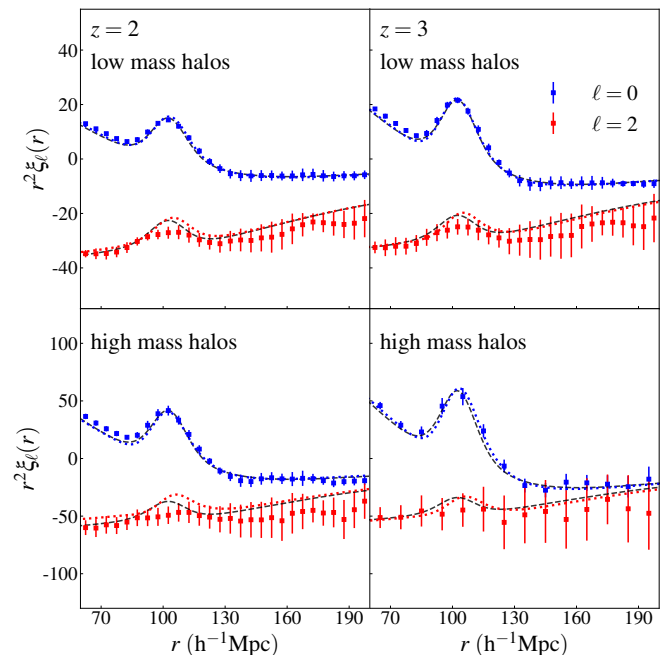


FIG. 1: Multipoles of redshift-space correlation functions of halos at  $z = 2$  (left) and  $z = 3$  (right). The upper and lower rows show the results for the low- and high-mass halos, respectively. The red and blue points are the measured monopole and quadrupole moments from  $N$ -body simulations. The dashed curves are the model with the input cosmological parameters. The dotted curves are the best-fitting model at  $60 \leq r \leq 200 h^{-1} \text{ Mpc}$  (see text). Errors are the square root of the diagonal components of the covariance matrices.

functions [40],

$$\xi_\ell(r) = (2\ell + 1) \int_0^1 \xi(r, \mu_r) \mathcal{L}_\ell(\mu_r) d\mu_r, \quad (1)$$

where  $\mathcal{L}_\ell(\mu_r)$  is the  $\ell$ -th order Legendre polynomials.

We need to estimate a covariance matrix for the measured correlation functions for cosmological analysis. We adopt a bootstrap resampling method [e.g., 41],

$$\begin{aligned} C_{ij} &\equiv C[\xi_\ell(r_i), \xi_{\ell'}(r_j)] \\ &= \frac{1}{N_{\text{mock}} - 1} \sum_{k=1}^{N_{\text{mock}}} [\xi_{\ell,k}(r_i) - \bar{\xi}_\ell(r_i)] \\ &\quad \times [\xi_{\ell',k}(r_j) - \bar{\xi}_{\ell'}(r_j)], \end{aligned} \quad (2)$$

where  $\xi_{\ell,k}(r_i)$  is the measurement from the  $k$ -th bootstrap realization and  $\bar{\xi}_\ell(r_i) = N_{\text{mock}}^{-1} \sum_{k=1}^{N_{\text{mock}}} \xi_{\ell,k}(r_i)$ . We create fifty realizations from each simulation. Furthermore, in measuring the redshift-space density field, we regard each direction along the three axes of simulation boxes as the line of sight. Thus, we have  $N_{\text{mock}} = 50 \times 3 \times 3 = 450$  realizations to construct the covariance matrix.

Fig. 1 shows both the monopole and quadrupole moments of the redshift-distorted-space correlation functions of redshift 2 and 3 halos for the high-mass and

low-mass bins. The error bars for the multipoles shown are the square root of the diagonal parts of the covariance matrix.

*Theoretical model.* Here we present a theoretical model of the correlation functions to place cosmological constraints. Since theoretical models are derived in Fourier space, we first consider a model for the redshift-space power spectrum,  $P(\mathbf{k}) = P(k, \mu_{\mathbf{k}})$ , with  $k = |\mathbf{k}|$  and  $\mu_{\mathbf{k}}$  the directional cosine. Given the underlying matter power spectrum in real space,  $P_m(k)$ , cosmological information is extracted from the dynamical and geometric distortions, which are probed, respectively, via RSD and Alcock-Paczynski (AP) effects [42–46].

We use the simplest model for RSD, the linear RSD model with a constant bias  $b$  [43]. It is given by

$$P(k, \mu_{\mathbf{k}}) = (b + f\mu_{\mathbf{k}}^2)^2 P_m(k), \quad (3)$$

where  $f(z)$  is the growth rate of the universe sensitive to modification of the gravity models and approximated by  $f(z) = \Omega_m^{6/11}(z)$  for the  $\Lambda$ CDM model. The BAO wiggles encoded in  $P_m(k)$  are damped due to the non-linear structure formation. Density-field reconstruction is widely used for increasing the precision and accuracy of the BAO detection [47, 48]. However, implementing the technique in full-shape analysis is non-trivial and different reconstruction methods would yield different constraints [49]. We instead adopt a conservative approach by including BAO damping in our model. Since the damping is less significant at high redshift, we include it using a simple model (e.g. [50]),

$$P_m(k) = P_{\text{nw}}(k) + [P_{\text{lin}}(k) - P_{\text{nw}}(k)] \exp\left(-\frac{k^2}{2k_*^2}\right), \quad (4)$$

where  $P_{\text{lin}}(k)$  and  $P_{\text{nw}}(k)$  are the linear matter power spectra with and without BAO wiggles, respectively [51]. The parameter  $k_*$  controls the effect of the damping. Although it can be computed analytically [52], we simply treat it as a free parameter and marginalize it over to obtain cosmological constraints.

Next, we consider the geometric distortion, the AP effect, induced by the apparent mismatch between the reference and true cosmology. This effect is modeled as

$$P^{\text{obs}}(k, \mu_{\mathbf{k}}) = \frac{H}{H_{\text{fid}}} \left( \frac{D_{\text{A, fid}}}{D_{\text{A}}} \right)^2 P(q, \nu_q), \quad (5)$$

where

$$q(k, \mu_{\mathbf{k}}) = \alpha(\mu_{\mathbf{k}})k, \quad \nu_q(k, \mu_{\mathbf{k}}) = \frac{1}{\alpha(\mu_{\mathbf{k}})} \frac{H}{H_{\text{fid}}} \mu_{\mathbf{k}}, \quad (6)$$

with  $\alpha(\mu_{\mathbf{k}})$  being

$$\alpha(\mu_{\mathbf{k}}) = \sqrt{\left( \frac{D_{\text{A, fid}}}{D_{\text{A}}} \right)^2 + \left[ \left( \frac{H}{H_{\text{fid}}} \right)^2 - \left( \frac{D_{\text{A, fid}}}{D_{\text{A}}} \right)^2 \right] \mu_{\mathbf{k}}^2}. \quad (7)$$

Here  $H(z)$  and  $D_{\text{A}}(z)$  are the expansion rate and angular diameter distance, respectively. Quantities with the subscript fid are computed using fiducial cosmological parameters (see Introduction). Detecting anisotropies of BAO enables us to separate the AP effect from the dynamical distortion effect.

Given  $P^{\text{obs}}(k, \mu_{\mathbf{k}})$ , the multipole moments are obtained as

$$P_{\ell}^{\text{obs}}(k) = (2\ell + 1) \int_0^1 P^{\text{obs}}(k, \mu_{\mathbf{k}}) \mathcal{L}_{\ell}(\mu_{\mathbf{k}}) d\mu_{\mathbf{k}}, \quad (8)$$

with  $\ell = 0, 2, 4$  containing cosmological information [53, 54]. These multipole power spectra can be converted into multipole correlation functions by

$$\xi_{\ell}(r) = i^{\ell} \int \frac{dk k^2}{2\pi^2} P_{\ell}^{\text{obs}}(k) j_{\ell}(kr), \quad (9)$$

where  $j_{\ell}$  is the  $\ell$ -th order spherical Bessel function.

In summary, given the matter power spectrum,  $P_m(k)$ , the measured redshift-space correlation function is characterized by a set of five parameters,  $\theta = (b(z), f(z), H(z), D_{\text{A}}(z), k_*)$ . The prediction with the input cosmological model for our simulations is shown by the black dashed curve in Fig. 1. Later in the paper, we perform direct constraints on cosmological parameters allowing the shape of the underlying power spectrum to vary, referred to as a full-shape analysis. For this case, the choice of the parameter space is arbitrary, and the above dynamical and geometric parameters are computed using the chosen parameters.

*Setup for cosmological analysis.* In this paper, we investigate how well one can constrain cosmological models at redshifts  $z > 2$  in two ways: (i) constrain the growth rate and expansion rate using dynamical and geometric distortions, (ii) constrain cosmological parameters directly by utilizing the cosmological dependence of the underlying power spectrum shape.

We perform the likelihood analysis using the measured correlation functions of the halos with the theoretical models described above. The  $\chi^2$  statistic is given by

$$\chi^2(\theta) = \sum_{i=1}^{N_{\text{bin}}} \sum_{j=1}^{N_{\text{bin}}} \Delta_i C_{ij}^{-1} \Delta_j, \quad (10)$$

where  $\Delta_i \equiv \Delta(r_i; \theta) = \xi_{\ell}^{\text{sim}}(r_i) - \xi_{\ell}^{\text{th}}(r_i; \theta)$  is the difference between the measured and predicted correlation functions, with  $\theta$  being a parameter set to be constrained. The analysis is performed on the adopted scales  $r_{\text{min}} \leq r_i \leq r_{\text{max}}$  with the number of bins for all multipole being  $N_{\text{bin}}$ . The degree of freedom is  $N_{\text{dof}} = N_{\text{bin}} - N_p$  with  $N_p$  the number of free parameters. The correlation functions on small scales are affected by various non-linear effects, namely non-linear evolution, RSD, and biasing. On the other hand, on large scales the covariance matrix is biased due to our resampling method. Thus, we use a conservative range for the likelihood analysis and set  $(r_{\text{min}}, r_{\text{max}}) = (60, 200) [h^{-1} \text{ Mpc}]$ . For this range,

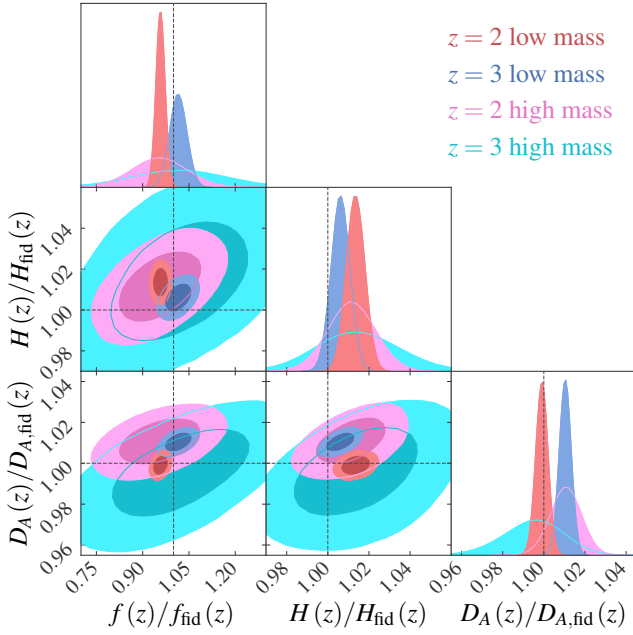


FIG. 2: Constraints on dynamical and geometric parameters,  $(f(z), H(z), D_A(z))$ , obtained by the correlation functions of low-/high-mass halos at  $60 \leq r \leq 200 h^{-1}$  Mpc. Nuisance parameters,  $b$  and  $k_*$ , are marginalized over. The contours show the 68% and 95% C.L. from inward.

the non-linearity of the matter power spectrum is completely negligible. We therefore compute  $P_m(k)$  in linear theory using the public code **CLASS** [55]. Since the non-linear RSD also does not significantly affect our result, we can safely use the linear RSD model (Eq. 3). Although the nonlinear bias effect is severer as we consider relatively massive halos, we still adopt the linear bias for simplicity. We set the bin size of the correlation function to  $\Delta r = 5 h^{-1}$  Mpc for both monopole and quadrupole, thus  $N_{\text{bin}} = 56$ , for all the halo samples except the high-mass halo sample at  $z = 3$  ( $\Delta r = 10 h^{-1}$  Mpc and  $N_{\text{bin}} = 28$ ) that is so sparse that the correlation function becomes noisy. To perform a maximum likelihood analysis we use the Markov Chain Monte Carlo sampler **emcee** [56], under flat priors otherwise stated.

Cosmological constraints obtained below correspond to those expected from a galaxy survey of the volume of our simulations,  $V = (2 h^{-1} \text{ Gpc})^3$ , smaller than typical upcoming surveys. However, since data in actual surveys are split into redshift bins for cosmological analysis, our constraints will roughly correspond to those from one redshift bin.

*Dynamical and geometric constraints.* For the analysis of dynamical and geometric distortions, we have five parameters in total,  $\theta = (b, f, H, D_A, k_*)$ , among which  $b$  and  $k_*$  are nuisance parameters that we want to marginalize over. The matter power spectrum is computed assuming the fiducial cosmology.

Fig. 2 shows two-dimensional error contours on the geometric and dynamical parameters for the four samples,

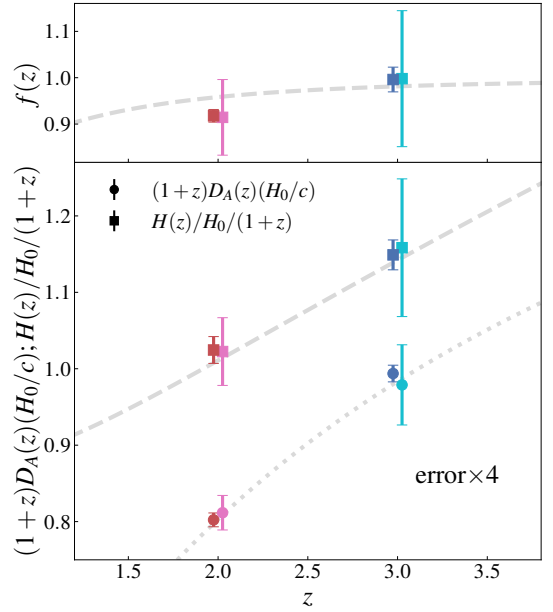


FIG. 3: One-dimensional marginalized errors on  $f(z)$  (upper panel) and  $H(z)$  and  $D_A(z)$  (lower panel) as functions of redshift. Gray curves are the true values of parameters at redshift 2 and 3. Errors of 68% confidence level are shown, but those on  $H$  and  $D_A$  are multiplied by 4 for illustration. For clarity, the results from the low- and high-mass halos are slightly offset horizontally toward left and right, respectively.

normalized by their fiducial values. Fig. 3 shows the one-dimensional marginalized errors as a function of redshift. The constrained parameters are summarized in Table II. The preliminary results of this analysis have been presented in [29]. The best-fit model obtained here is shown by the dotted curves in Fig. 1.

Since the simulation box size is fixed, the strength of the constraints depends on the number density of halo samples. The best-fit models are consistent with the input (true) models of the simulations within  $2\sigma$  level except for the low-mass sample at  $z = 2$ . This offset is caused by the fact that our simple linear model is not very accurate for the precision measurement. Furthermore, this model provides a poor fit for this sample with the reduced  $\chi^2$  value of  $\chi^2_{\text{min}}/N_{\text{dof}} \approx 4$ . However, such systematic effects can be easily controlled once a more sophisticated model (e.g., [57, 58]). The precision of the growth rate is at most 15% for low number density and high mass halos. The precision is significantly improved to  $\sim 2 - 3\%$  as the number density increases to a few times  $10^{-3} h^3 \text{ Mpc}^{-3}$ . We see a similar trend for  $H(z)$  and  $D_A(z)$ , whose constraints improve from 1.9% to 0.4% and 1.3% to 0.3%, respectively. The Lyman- $\alpha$  survey result in the DESI Collaboration [12] gives 2% and 2.4% precision in  $H(z)$  and  $D_A(z)$ , respectively, with number density  $n_g = 3 \times 10^{-5} h^3 \text{ Mpc}^{-3}$  at effective redshift 2.33. Our results at  $z = 2$  are, therefore, confirmed by obser-

TABLE II: Dynamical and geometric parameter constraints.

$\theta$	$z = 2$			$z = 3$		
	fiducial	low mass	high mass	fiducial	low mass	high mass
$f$	0.958	$0.918^{+0.014}_{-0.013}$	$0.914^{+0.082}_{-0.082}$	0.981	$0.996^{+0.027}_{-0.027}$	$0.998^{+0.147}_{-0.147}$
$D_A$	1193.3	$1192.1^{+3.4}_{-3.4}$	$1206.0^{+8.4}_{-8.6}$	1096.0	$1107.4^{+3.0}_{-3.0}$	$1090.9^{+14.6}_{-16.1}$
$H$	204.09	$206.85^{+0.89}_{-0.86}$	$206.44^{+2.24}_{-2.23}$	307.43	$309.31^{+1.32}_{-1.32}$	$311.84^{+6.06}_{-5.76}$
$b$		$1.942^{+0.015}_{-0.015}$	$3.365^{+0.099}_{-0.103}$		$3.238^{+0.025}_{-0.025}$	$5.514^{+0.176}_{-0.178}$
$\chi^2_{\min}/N_{\text{dof}}$		206.063/51	48.069/51		129.219/51	14.976/23

variations.

*Full-shape constraints.* Here we utilize the cosmological information encoded in the underlying matter power spectrum and directly constrain cosmological parameters. We consider a nonflat  $\Lambda$ CDM model with six parameters in total,  $\theta = (b, \Omega_m, \Omega_k, H_0, A_s, k_*)$ , where  $A_s$  is the amplitude of the primordial curvature perturbations. We fix the baryon density,  $\omega_b \equiv \Omega_b h^2$ , to the fiducial value because it is tightly constrained by CMB and big-bang nucleosynthesis [2, 59, 60]. We further fix the dark energy equation-of-state to a cosmological constant,  $w_0 = -1$ , as the high- $z$  clustering is not sensitive to  $w$ . On the other hand, the high-redshift universe is a useful laboratory to test the flatness of the universe,  $\Omega_k$  [16].

Since there is a strong degeneracy between  $b$  and  $A_s$  in linear theory, they cannot be tightly constrained [46]. For sampling stability and efficiency of the MCMC, we adopt a Gaussian prior on  $A_s$  and marginalize it over together with the other nuisance parameters,  $b$  and  $k_*$ . We confirmed that this does not affect constraints on the other parameters, since the degeneracies between  $A_s$  and other parameters are relatively small.<sup>1</sup> Here we exclude  $z = 2$  low-mass halo samples from our discussion, as our model of the correlation function is too simple to provide accurate cosmological constraints via the full-shape analysis from them.

Fig. 4 shows the two-dimensional constraints on pairs of cosmological parameters. Table III summarizes the one-dimensional marginalized constraints. The best-fitting value of  $b$  obtained here is fully consistent with that from dynamical and geometric constraints. We obtain 0.7 – 2.5% constraints on  $\Omega_m$  and 0.5 – 1.7% on  $H_0$ . The reported discrepancy between the values of  $H_0$  measured using early and late universe probes is about 5 – 10% [10]. Our result thus demonstrates that achieving the number density of  $\bar{n}_g \simeq 10^{-4} (h^3 \text{ Mpc}^{-3})$  over

the large volume at  $z \geq 2$  provides a powerful test of the Hubble tension, independent of the local universe ( $z \simeq 0$ ) and early universe ( $z \simeq 1100$ ) measurements.

Note that there are certain offsets for the constraint on  $\Omega_m$  from the  $z = 2$  sample, though  $\simeq 2\sigma$ , while the results shown in the previous subsection are consistent with the input within the  $1\sigma$  level for these samples. These shifts are driven by the inaccuracy of our linear theory model with the simple BAO damping on small scales, where cosmological information can still be extracted. In fact, Fig. 1 shows that the best-fit model fails to capture behavior on smaller scales than the BAO scale, especially at  $z = 2$ , while it agrees with the measurements up to the BAO scale. This issue can be easily restored once one employs a more sophisticated model, and our main

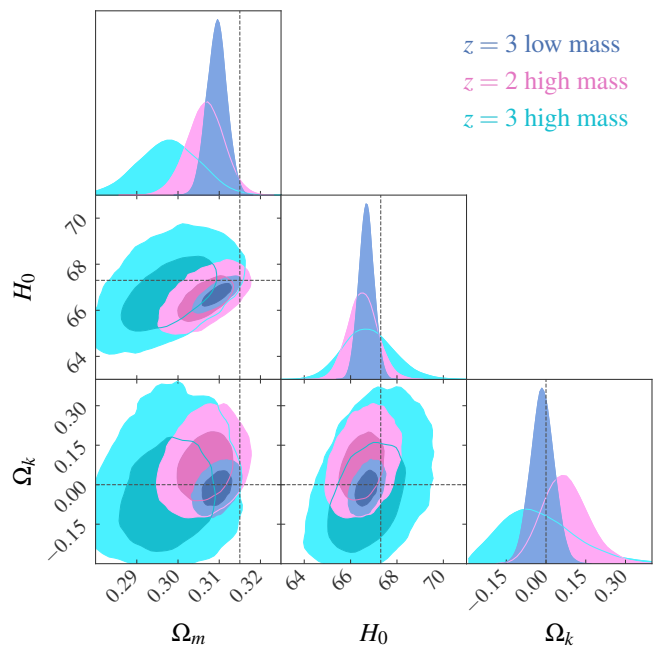


FIG. 4: Constraints on cosmological parameters ( $\Omega_m, H_0, \Omega_k$ ) from the full-shape information of correlation functions of high-mass halo samples at  $z = 2$ , as well as low-/high-mass halo samples at  $z = 3$ . Nuisance parameters,  $b$  and  $k_*$ , as well as the amplitude  $A_s$  are marginalized over. The dotted lines indicate the fiducial values.

<sup>1</sup> Using the shape information of the power spectrum on nonlinear scales and the bispectrum enables one to simultaneously determine  $b$  and the perturbation amplitude, and thus to investigate the  $\sigma_8$  (or  $S_8$ ) tension [61]. Such an investigation is left to our future work.

TABLE III: Cosmological parameter constraints.

$\theta$	fiducial	$z = 2$	$z = 3$	
		high mass	low mass	high mass
$\Omega_m$	0.3150	$0.3067^{+0.0043}_{-0.0045}$	$0.3095^{+0.0023}_{-0.0024}$	$0.2977^{+0.0074}_{-0.0076}$
$H_0$	67.30	$66.52^{+0.63}_{-0.62}$	$66.68^{+0.32}_{-0.32}$	$66.74^{+1.12}_{-1.02}$
$\Omega_k$	0	$0.070^{+0.088}_{-0.080}$	$-0.014^{+0.044}_{-0.043}$	$-0.039^{+0.158}_{-0.125}$
$10^9 A_s$	2.12	$2.12^{+0.11}_{-0.11}$	$2.14^{+0.11}_{-0.11}$	$2.12^{+0.10}_{-0.10}$
$b$		$3.373^{+0.227}_{-0.218}$	$3.106^{+0.087}_{-0.086}$	$5.170^{+0.517}_{-0.452}$
$\chi^2_{\min}/N_{\text{dof}}$		54.557/50	123.761/50	11.985/22

conclusion of constraining cosmology from high redshifts is unchanged. Small discrepancies of the quadrupoles around the BAO scales will be further improved by including the angle-dependent BAO damping.

We also obtain interesting constraints on the spatial curvature at both redshifts. Using the Fisher matrix formalism, Ref. [16] showed that one can achieve the precision of  $|\Omega_k| \lesssim 3 \times 10^{-3}$  (68% C.L.) by observing all the galaxies with  $10^{-4} (h^3 \text{ Mpc}^{-3})$  at  $0 \leq z \leq z_{\text{max}}$  where  $z_{\text{max}} \simeq 2$ , which is the most optimistic and ideal situation. With more realistic simulation-based analysis, we show that the galaxy clustering at one-single redshift of  $z = 2$  or  $z = 3$  provides a constraint on  $\Omega_k$ , as  $|\Omega_k| \lesssim 0.1$ , without relying on other observations such as the CMB.

*Summary and discussion.* In this paper, we have studied the cosmological constraints expected from upcoming high-redshift galaxy surveys utilizing high-resolution  $N$ -body simulations at  $z = 2$  and  $3$ . To obtain general conclusions, we did not consider specific galaxy populations or survey geometries but rather split our halo sample into low-mass and high-mass subsamples in a cubic box of side  $2 h^{-1} \text{ Gpc}$ . We chose a conservative fitting range where a simple linear theory prediction recovered the input cosmological models. We considered two analysis methods, a template fitting for dynamical and geometric constraints and a full-shape analysis. With the former, we obtained a  $\sim 15\%$  constraint on  $f(z)$  with the massive halo sample with  $\bar{n}_g \sim 10^{-4} h^3 \text{ Mpc}^{-3}$  but the constraint improved to a few percent by increasing the number density by an order of magnitude. On the other hand, we achieved  $< 2\%$  constraints on  $H(z)$  and  $D_A(z)$  even with the low-number density halo sample. Our full-shape analysis demonstrated that we can simultaneously investigate the Hubble tension and the flatness of the universe. Including the nonlinearity of the matter spectrum further enables us to address the  $\sigma_8$  (or  $S_8$ ) tension without combining the CMB priors.

Our analyses provide a timely forecast for the upcoming spectroscopic surveys. For example, the expected

number density for the emission line galaxy (ELG) sample in PFS at redshift 2 is  $2.7 \times 10^{-4} h^3 \text{ Mpc}^{-3}$  [25]. With already good precision in DESI's results including galaxies spanning on a larger range of redshifts with a much lower number density of our samples, we can expect to see percent or sub-percent level constraints on cosmological parameters in PFS or future DESI releases that have higher number density. Our forecasts on massive halos are also helpful in guiding the design of the AtLAST spectroscopic surveys, which will predominantly target dusty star-forming galaxies at  $z \gtrsim 2$ . The expected number density obtained from AtLAST is comparable to those of both of our high-mass bins, which, based on our results, will allow for percent levels of constraints on cosmological parameters.

This paper did not consider any specific galaxy sample or survey geometry. For a more realistic cosmological forecast based on simulations, we need to generate light-cone output using multiple snapshots of  $N$ -body simulations (e.g., [62, 63]). Although the halo occupation distribution (HOD) of ELGs has been studied recently (e.g., [64, 65]), that of dusty galaxies still contains several uncertainties. Thus, a cosmological forecast for dusty galaxies at high redshifts requires more effort. Such detailed investigations and analyses will be performed in our future work.

*Acknowledgments.* TO acknowledges support of the Taiwan National Science and Technology Council under Grants No. NSTC 112-2112-M-001-034-, NSTC 113-2112-M-001-011- and NSTC 114-2112-M-001-004-, and the Academia Sinica Investigator Project Grant No. AS-IV-114-M03 for the period of 2025–2029. SYP and CCC acknowledge the support of the Taiwan National Science and Technology Council (111-2112M-001-045-MY3), as well as the Academia Sinica through the Career Development Award (AS-CDA-112-M02). TN acknowledges support by JSPS KAKENHI Grant Numbers JP20H05861, JP21H01081, JP22K03634, JP24H00215 and JP24H00221. KA is supported by Fostering Joint International Research (B) under Contract No. 21KK0050 and the Japan Society for the Promotion of Science (JSPS) KAKENHI Grant No. JP24K17056. We acknowledge ‘the HPC facility at ASIAA’ where part of the numerical analyses were done. This work used high-performance computing facilities operated by the Center for Informatics and Computation in Astronomy (CICA) at National Tsing Hua University. This equipment was funded by the Ministry of Education of Taiwan, the Ministry of Science and Technology of Taiwan, and National Tsing Hua University. We are grateful to the maintenance and administrative staff of our institutions, whose efforts in supporting our day-to-day work environment make our scientific discoveries possible.

[1] G. Hinshaw, D. Larson, E. Komatsu, D. N. Spergel, C. L. Bennett, J. Dunkley, M. R. Nolta, M. Halpern, R. S. Hill,

N. Odegard, et al., *Astrophys. J. Suppl.* **208**, 19 (2013)

- [2] Planck Collaboration, P. A. R. Ade, N. Aghanim, M. Arnaud, M. Ashdown, J. Aumont, C. Baccigalupi, A. J. Banday, R. B. Barreiro, J. G. Bartlett, et al., *Astron. Astrophys.* **594**, A13 (2016)
- [3] T. M. C. Abbott, F. B. Abdalla, A. Alarcon, J. Aleksić, S. Allam, S. Allen, A. Amara, J. Annis, J. Asorey, S. Avila, et al., *Phys. Rev. D* **98**, 043526 (2018)
- [4] C. Hikage, M. Oguri, T. Hamana, S. More, R. Mandelbaum, M. Takada, F. Köhlinger, H. Miyatake, A. J. Nishizawa, H. Aihara, et al., *Publ. Astron. Soc. Jpn.* **71**, 43 (2019)
- [5] M. M. Ivanov, M. Simonović, and M. Zaldarriaga, *JCAP* **5**, 042 (2020)
- [6] G. d’Amico, J. Gleyzes, N. Kokron, K. Markovic, L. Senatore, P. Zhang, F. Beutler, and H. Gil-Marín, *JCAP* **5**, 005 (2020)
- [7] Y. Kobayashi, T. Nishimichi, M. Takada, and H. Miyatake, *Phys. Rev. D* **105**, 083517 (2022)
- [8] N. Suzuki, D. Rubin, C. Lidman, G. Aldering, R. Amanullah, K. Barbary, L. F. Barrientos, J. Botyanszki, M. Brodwin, N. Connolly, et al., *Astrophys. J.* **746**, 85 (2012)
- [9] T. M. C. Abbott, M. Acevedo, M. Agüena, A. Alarcon, S. Allam, O. Alves, A. Amon, F. Andrade-Oliveira, J. Annis, P. Armstrong, et al., *Astrophys. J. Lett.* **973**, L14 (2024)
- [10] L. Verde, T. Treu, and A. G. Riess, *Nature Astronomy* **3**, 891 (2019)
- [11] E. Abdalla, G. F. Abellán, A. Aboubrahim, A. Agnello, Ö. Akarsu, Y. Akrami, G. Alestas, D. Aloni, L. Amendola, L. A. Anchordoqui, et al., *Journal of High Energy Astrophysics* **34**, 49 (2022)
- [12] A. G. Adame, J. Aguilar, S. Ahlen, S. Alam, D. M. Alexander, M. Alvarez, O. Alves, A. Anand, U. Andrade, E. Armengaud, et al., *JCAP* **1**, 124 (2025)
- [13] A. G. Adame, J. Aguilar, S. Ahlen, S. Alam, D. M. Alexander, M. Alvarez, O. Alves, A. Anand, U. Andrade, E. Armengaud, et al., *JCAP* **4**, 012 (2025)
- [14] DESI Collaboration, A. G. Adame, J. Aguilar, S. Ahlen, S. Alam, D. M. Alexander, M. Alvarez, O. Alves, A. Anand, U. Andrade, et al., *JCAP* **2**, 021 (2025)
- [15] S. Roy Choudhury and T. Okumura, *Astrophys. J. Lett.* **976**, L11 (2024)
- [16] M. Takada and O. Doré, *Phys. Rev. D* **92**, 123518 (2015)
- [17] R. Terasawa, R. Takahashi, T. Nishimichi, and M. Takada, *Phys. Rev. D* **106**, 083504 (2022)
- [18] S. Anselmi, M. F. Carney, J. T. Giblin, S. Kumar, J. B. Mertens, M. O’Dwyer, G. D. Starkman, and C. Tian, *JCAP* **2**, 049 (2023)
- [19] J. Stevens, H. Khoraminezhad, and S. Saito, *JCAP* **7**, 046 (2023)
- [20] R. Terasawa, R. Takahashi, T. Nishimichi, and M. Takada, *Phys. Rev. D* **109**, 063504 (2024)
- [21] T. Okumura, C. Hikage, T. Totani, M. Tonegawa, H. Okada, K. Glazebrook, C. Blake, P. G. Ferreira, S. More, A. Taruya, et al., *Publ. Astron. Soc. Jpn.* **68**, 38 (2016)
- [22] M. Takada, E. Komatsu, and T. Futamase, *Phys. Rev. D* **73**, 083520 (2006)
- [23] C. Dvorkin, M. Gerbino, D. Alonso, N. Battaglia, S. Bird, A. Diaz Rivero, A. Font-Ribera, G. Fuller, M. Lattanzi, M. Loverde, et al., *BAAS* **51**, 64 (2019)
- [24] S. Ferraro and M. J. Wilson, *BAAS* **51**, 72 (2019)
- [25] M. Takada, R. S. Ellis, M. Chiba, J. E. Greene, H. Aihara, N. Arimoto, K. Bundy, J. Cohen, O. Doré, G. Graves, et al., *Publ. Astron. Soc. Jpn.* **66**, R1 (2014)
- [26] J. Marshall, A. Bolton, J. Bullock, A. Burgasser, K. Chambers, D. DePoy, A. Dey, N. Flagey, A. Hill, L. Hillenbrand, et al., in *Bulletin of the American Astronomical Society* (2019), vol. 51, p. 126
- [27] D. J. Schlegel, J. A. Kollmeier, G. Aldering, S. Bailey, C. Baltay, C. Bebek, S. BenZvi, R. Besuner, G. Blanc, A. S. Bolton, et al., *arXiv e-prints arXiv:2209.04322* (2022)
- [28] R. Ellis and K. Dawson, in *Bulletin of the American Astronomical Society* (2019), vol. 51, p. 45
- [29] E. van Kampen, T. Bakx, C. De Breuck, C.-C. Chen, H. Dannerbauer, B. Magnelli, F. M. Montenegro-Montes, T. Okumura, S.-Y. Pu, M. Rybak, et al., *Open Research Europe* **4**, 122 (2024)
- [30] A. A. Khostovan, D. Sobral, B. Mobasher, J. Matthee, R. K. Cochrane, N. Chartab, M. Jafariyazani, A. Paulino-Afonso, S. Santos, and J. Calhau, *Mon. Not. Roy. Astron. Soc.* **489**, 555 (2019)
- [31] C.-F. Lim, C.-C. Chen, I. Smail, W.-H. Wang, W.-L. Tee, Y.-T. Lin, D. Scott, Y. Toba, Y.-Y. Chang, Y. Ao, et al., *Astrophys. J.* **895**, 104 (2020)
- [32] S. M. Stach, I. Smail, A. Amvrosiadis, A. M. Swinbank, U. Dudzevičiūtė, J. E. Geach, O. Almaini, J. E. Birkin, C.-C. Chen, C. J. Conselice, et al., *Mon. Not. Roy. Astron. Soc.* **504**, 172 (2021)
- [33] P. McDonald and U. Seljak, *JCAP* **10**, 007 (2009)
- [34] H. Ebina and M. White, *JCAP* **6**, 052 (2024)
- [35] T. Okumura and A. Taruya, *Phys. Rev. D* **106**, 043523 (2022)
- [36] S. Ilić, N. Aghanim, C. Baccigalupi, J. R. Bermejo-Clement, G. Fabbian, L. Legrand, D. Paoletti, M. Ballardini, M. Archidiacono, M. Douspis, et al., *Astronomy & Astrophysics* **657**, A91 (2022).
- [37] W. d’Assignies D, C. Zhao, J. Yu, and J.-P. Kneib, *Monthly Notices of the Royal Astronomical Society* **521**, 3648–3662 (2023).
- [38] T. Nishimichi, M. Takada, R. Takahashi, K. Osato, M. Shirasaki, T. Oogi, H. Miyatake, M. Oguri, R. Murata, Y. Kobayashi, et al., *Astrophys. J.* **884**, 29 (2019)
- [39] P. S. Behroozi, R. H. Wechsler, and H.-Y. Wu, *Astrophys. J.* **762**, 109 (2013)
- [40] A. J. S. Hamilton, *Astrophys. J. Lett.* **385**, L5 (1992).
- [41] P. Norberg, C. M. Baugh, E. Gaztañaga, and D. J. Croton, *Mon. Not. Roy. Astron. Soc.* **396**, 19 (2009)
- [42] C. Alcock and B. Paczynski, *Nature (London)* **281**, 358 (1979).
- [43] N. Kaiser, *Mon. Not. Roy. Astron. Soc.* **227**, 1 (1987).
- [44] H.-J. Seo and D. J. Eisenstein, *Astrophys. J.* **598**, 720 (2003)
- [45] T. Matsubara, *Astrophys. J.* **615**, 573 (2004)
- [46] T. Okumura, T. Matsubara, D. J. Eisenstein, I. Kayo, C. Hikage, A. S. Szalay, and D. P. Schneider, *Astrophys. J.* **676**, 889–898 (2008)
- [47] D. J. Eisenstein, H.-J. Seo, E. Sirko, and D. N. Spergel, *Astrophys. J.* **664**, 675 (2007)
- [48] E. Paillas, Z. Ding, X. Chen, H. Seo, N. Padmanabhan, A. de Mattia, A. J. Ross, S. Nadathur, C. Howlett, J. Aguilar, et al., *JCAP* **1**, 142 (2025)
- [49] W. Zhang, R. Zhao, X. Mu, K. Koyama, R. Takahashi, Y. Wang, and G.-B. Zhao, *arXiv e-prints arXiv:2503.20574* (2025)



- [50] C.-H. Chuang and Y. Wang, *Mon. Not. Roy. Astron. Soc.* **431**, 2634 (2013)
- [51] D. J. Eisenstein and W. Hu, *Astrophys. J.* **496**, 605 (1998)
- [52] Z. Vlah, U. Seljak, M. Yat Chu, and Y. Feng, *JCAP* **3**, 057 (2016)
- [53] S. Cole, K. B. Fisher, and D. H. Weinberg, *Mon. Not. Roy. Astron. Soc.* **267**, 785 (1994)
- [54] T. Okumura and Y. P. Jing, *Astrophys. J.* **726**, 5 (2011)
- [55] D. Blas, J. Lesgourgues, and T. Tram, *JCAP* **7**, 034 (2011)
- [56] D. Foreman-Mackey, D. W. Hogg, D. Lang, and J. Goodman, *Publ. Astron. Soc. Pac.* **125**, 306 (2013)
- [57] T. Nishimichi, G. D’Amico, M. M. Ivanov, L. Senatore, M. Simonović, M. Takada, M. Zaldarriaga, and P. Zhang, *Physical Review D* **102** (2020).
- [58] S.-F. Chen, Z. Vlah, E. Castorina, and M. White, *JCAP* **3**, 100 (2021)
- [59] E. Aver, K. A. Olive, R. L. Porter, and E. D. Skillman, *JCAP* **11**, 017 (2013)
- [60] R. Cooke, M. Pettini, R. A. Jorgenson, M. T. Murphy, and C. C. Steidel, *Astrophys. J.* **781**, 31 (2014)
- [61] O. H. E. Philcox and M. M. Ivanov, *Phys. Rev. D* **105**, 043517 (2022)
- [62] C. Howlett, M. Manera, and W. J. Percival, *Astronomy and Computing* **12**, 109 (2015)
- [63] S. Ishikawa, T. Okumura, and T. Nishimichi, *Mon. Not. Roy. Astron. Soc.* **529**, 1839 (2024)
- [64] S. Avila, V. Gonzalez-Perez, F. G. Mohammad, A. de Mattia, C. Zhao, A. Raichoor, A. Tamone, S. Alam, J. Bautista, D. Bianchi, et al., *Mon. Not. Roy. Astron. Soc.* **499**, 5486 (2020)
- [65] T. Okumura, M. Hayashi, I. N. Chiu, Y.-T. Lin, K. Osato, B.-C. Hsieh, and S.-C. Lin, *Publ. Astron. Soc. Jpn.* **73**, 1186 (2021)